Adsorption, Structure, and Dynamics of Short- and Long-Chain PFAS Molecules in Kaolinite: Molecular Level Insights

Narasimhan Loganathan[*] *and Angela K. Wilson*[*]

Department of Chemistry, Michigan State University, East Lansing, Michigan 48824, United States

[*]) **Corresponding author's e-mail:** akwilson@msu.edu

naresh20@msu.edu

Abstract

The ubiquitous presence of poly- and perfluoroalkyl substances (PFAS) in different natural settings pose a serious threat to environmental and human health. Soils and sediments represent one of the important exposure pathways of PFAS for humans and animals. With increasing bioaccumulation and mobility, it is extremely important to understand the interactions of PFAS molecules with the dominant constituents of soils such as clay minerals. This study reports for the first time the fundamental molecular level insights into the adsorption, interfacial structure, and dynamics of short- and long-chain PFAS molecules at the water saturated mesopores of kaolinite clay using classical molecular dynamics (MD) simulations. At environmental conditions, all the PFAS molecules are exclusively adsorbed near the hydroxyl surface of the kaolinite, irrespective of the terminal functional groups and metal cations. The interfacial adsorption structures and coordination environments of PFAS is strongly dependent on the nature of the functional groups and their hydrophobic chain length. The formation of large, aggregated clusters of long-chain PFAS at the hydroxyl surface of kaolinite is responsible for their restricted dynamics in comparison to short-chain PFAS molecules. Such comprehensive knowledge of PFAS at the clay mineral interface is critical to developing novel site-specific degradation and mitigation strategies.

Synopsis

This study provides critical insight about the fate and transport of PFAS contaminants in soils and sediments.

Keywords

Kaolinite, PFOA, PFOS, Diffusion, PFAS distribution, Soils.

Introduction

Poly- and perfluoroalkyl substances (PFAS) often known as "forever chemicals" have been classified as critical emerging contaminants due to reported detrimental effects of certain PFAS molecules on the environment and human health.[1–8] PFAS represents a class of >9000 molecules that exhibits unique hydrophobic and lipophobic properties, thus enabling them to be widely incorporated in a myriad of industrial, commercial, and domestic applications for well over five decades. Uses of PFAS include non-stick cookware, firefighting foams, food packaging, paints, cosmetics, pesticides, water resistant cloth, and carpets. The ubiquitous presence of PFAS in various natural settings originates from their strong C-F bonds which provides them extreme stability and hence enables them to be resistant to photolytic, biological and chemical degradation.[9,10] Consequently, human exposure to PFAS is inevitable and has been linked to adverse health impacts such as carcinogenesis, neurotoxicity, cardiovascular diseases, developmental and reproductive disorders.[8,11–16] In recent studies, we demonstrated the binding of short- and long-chain PFAS molecules to two important nuclear receptors which are responsible for regulating drug interactions and glucose metabolism.[17,18]

Studies by Ahrens et al.[19,20] clearly highlighted that soils and sediments represent important pathways for direct and indirect exposure of PFAS to ecosystems. In fact, a number of studies have assessed the sorption behavior of PFAS in field soil samples.[21–29] These studies clearly highlight that the sorption of PFAS is greatly influenced by soil composition. Consequently, huge efforts towards the development of novel adsorbent materials have been pursued, which show varying levels of success for the effective treatment and removal of PFAS from soil matrices.[10,30–35] However, complete elimination of PFAS from soils and sediments is still not possible which could be attributed to poor understanding of the critical roles exerted by the different components of

68 soils. For instance, the influence of clay minerals, the prominent components of soils, and the
69 prevalent metal cations on the fate and transport of PFAS in near- and sub-surface regions is poorly
70 understood. Such fundamental insights are extremely important as both clay minerals and metal
71 cations have been shown to greatly alter the distribution of other organic and inorganic species in
72 natural settings.[36–42] Therefore, a systematic investigation of the adsorption and mobility of PFAS
73 with different clay minerals varying in structural composition is of high importance. Furthermore,
74 the accurate evaluation of the sorption characteristics of PFAS by constituents in soils will provide
75 a route to make further progress in the mitigation strategies.

76 To date, there is only a limited number of batch adsorption experimental studies on PFAS
77 in clays.[43–50] For instance, Xiao et al.[43] reported that the adsorption of perfluorooctane sulfonic
78 acid (PFOS) is much higher than for perfluorooctanoic acid (PFOA) in kaolinite clay mineral.
79 More importantly, recent studies demonstrated that the adsorption of PFAS molecules with
80 sulfonate and carboxylate functional groups is ten times higher in kaolinite than in smectite
81 mineral, montmorillonite.[45,46] In addition, Zhang et al.[46] reported that PFAS adsorption is strongly
82 influenced by metal cations in clay minerals. On the other hand, Zhao et al.[47] showed that the
83 adsorption of short-chain PFAS molecules is more limited than that of long-chain PFAS in both
84 kaolinite and montmorillonite. Studies based on conceptual and transport models have indicated
85 that short-chain PFAS molecules are highly mobile and exhibit long-range transport when
86 compared to long-chain molecules.[51,52] Despite progress in the macroscopic understanding of the
87 adsorption process, a molecular level understanding is completely unexplored in areas including
88 the role of clay composition in dictating the specific adsorption and structural environments of
89 PFAS at the interface, the variance of the surface coordination characteristics of PFAS with respect
90 to clay substrates, and the pivotal fundamental interactions that govern the adsorption and

91 dynamics of PFAS in clay minerals. To our knowledge, there is only one computational study that
92 focused on the adsorption of PFAS in nanoconfined pores of montmorillonite – this study showed
93 that the adsorption is influenced by both the surface charge of the clay minerals and the length of
94 the PFAS molecules.[53]

95 The current study is focused to unravel the underlying factors that instigate the adsorption
96 and dynamics of PFAS in a clay mineral that is abundantly present in soils and sediments, namely
97 kaolinite for the first time. It represents a 1:1 layered silicate mineral and is composed of a layer
98 of Si tetrahedra connected to one Al octahedral layer. Importantly, the presence of three hydroxyl
99 groups at the basal surface of the octahedral layer in kaolinite results in a hydrophilic character
100 while the basal surface of Si tetrahedra exhibits a hydrophobic behavior. These unique
101 hydrophobic and hydrophilic surface characteristics of kaolinite could play a critical role during
102 the adsorption and transport of PFAS molecules, which also have a hydrophobic backbone and a
103 polar group with different functionalities. Prior work on kaolinite has considered the adsorption of
104 highly polar organic molecules including citric acid, decahydro-2-naphthoic acid and methanol at
105 the basal surfaces using molecular dynamics (MD) simulations.[54,55]

106 The main objective of this investigation is to gain a detailed molecular level understanding
107 of the adsorption, structure and dynamics of four different PFAS molecules at the H_2O saturated
108 mesopores of kaolinite at ambient thermodynamic conditions using MD simulations. Importantly,
109 this study provides mechanistic insight about the interfacial properties of PFAS in kaolinite under
110 three different scenarios: (i) molecules with similar length but with different terminal functional
111 groups (carboxylic and sulfonic acids); (ii) short- and long-chain PFAS molecules having same
112 functional groups; (iii) presence of naturally prevalent metal cations (K^+, Na^+, Ca^{2+}).

113 **Simulation Details**

The structure of kaolinite used in this study is based on the optimized structure from Cygan et al.[56] and has a structural formula of $Al_2Si_2O_5(OH)_4$. The hydrogen bonding interactions between the hydroxyl groups associated with Al octahedra and the basal surface oxygen atoms of the adjacent Si tetrahedra (siloxane) are responsible for the formation of kaolinite particles. The external kaolinite surface was constructed by cleaving the structure along the (001) plane which results in both the siloxane surface and the hydroxyl surface of kaolinite exposed to interact with the bulk solution phase. The simulation cell consisted of two kaolinite layers and a nanopore region of ~136 Å bound by the cleaved surfaces (Figure 1). The lateral (x and y) dimensions of the simulation cell correspond to ~62 Å and ~72 Å while the total initial length along z direction was ~150 Å with a total of 192 unit cells. The large nanopore thickness normal to the kaolinite (001) surface effectively eliminated any interactions of hydroxyl surface over adjacent siloxane surface when the periodic boundary conditions were applied and hence generated two statistically independent interparticle interfaces. In addition, the large surface area along with the nanopore region provided sufficient space for the PFAS molecules to move and interact with the cleaved surfaces and among themselves. The external (001) surface was initially saturated with ~20,000 water molecules at ambient conditions and 16 PFAS molecules. Four different PFAS molecules, namely perfluorobutanoic acid (PFBA), perfluorobutane sulfonic acid (PFBS), perfluorooctanoic acid (PFOA) and perfluorooctane sulfonic acid (PFOS) were examined that vary both in terminal functional groups and length of the hydrophobic carbon backbone. Importantly, the PFAS molecules examined represent both short- (PFBA and PFBS) and long-chain (PFOA and PFOS) entities that exhibit completely different adsorption and transport properties in experiments.[43,46,52] In a given simulated model, a total of 16 PFAS molecules (representing one of the four PFAS types) were initially placed at four distinct regions with a separation of 20 Å between the regions

137 (Figure 1). Moreover, in any given region the four PFAS molecules were placed with ~15-20 Å
138 separation between each other. To simulate near-neutral pH conditions, the terminal functional
139 groups (carboxylic/sulfonic acids) of PFAS molecules were deprotonated. Consequently, metal
140 cations were included in the nanopore region to charge compensate the anionic PFAS. The
141 influence of metal cations on the adsorption and dynamics of PFAS was examined with K^+, Na^+
142 and Ca^{2+} ions that exhibits completely different size/charge ratio and hydration properties and are
143 commonly identified in surface waters and clay minerals. Similar to the approach for the PFAS
144 molecules, the metal cations were placed throughout the nanopore region and away from both
145 PFAS and one another, thus allowing the preferred adsorption environments to be determined
146 during the course of the simulation. Thus, a total of 12 simulation models were investigated in this
147 study. Importantly, it should be noted that the concentrations of PFAS used in this study are in the
148 ppm range and are representative of contaminated sites around air force base and military
149 installations across United States as shown in studies by Brusseau et al.[27]

150 All classical molecular dynamics simulations were performed using the LAMMPS simulation
151 package.[57] All kaolinite models were simulated initially in the *NPT* ensemble (constant number of
152 atoms *N*, constant pressure *P*, and constant temperature *T*) and subsequently in the *NVT* ensemble
153 (constant number of atoms *N,* constant volume, *V,* and constant temperature *T*) at ambient
154 thermodynamic conditions (T=300 K, P=1 bar). A Nose-Hoover thermostat and barostat were used
155 to control the temperature and pressure separately in all three dimensions.[58,59] Three dimensional
156 periodic boundary conditions were employed with a cutoff distance of 9.0 Å for the calculation of
157 short-range non-electrostatic interactions, and the long-range electrostatics were computed using
158 the particle-particle-particle-mesh (PPPM) summation algorithm with an accuracy of 10^{-6}.[60] The
159 interatomic interactions for the kaolinite and metal cations were obtained from the ClayFF force

field in combination with newly developed metal-O-H bending potentials that are consistent with ClayFF.[56,61,62] The interactions of the H_2O and PFAS molecules were modeled with the flexible SPC[63] interaction potential and AMBER force field,[64,65] respectively. These interaction potentials are extensively used in clay interfacial simulations,[66–69] organic-mineral complexation[70–72] and material sciences studies that corroborate well with experiments.[73–76] The partial charges for the atoms in all four different PFAS molecules were computed using the AM1-BCC charge generation scheme with the Antechamber module.[65,77,78] A time step of 1 fs was used to integrate the equations of motion. For each modeled system, NPT simulations were performed for 15 ns entailing 10 ns of equilibration and 5 ns of data production, with data recorded every 10 fs. The equilibrium cell dimensions were calculated using the last 3 ns of the production run with 10 equal time blocks (300 ps each), yielding small errors for the reported mean values (Table S1). NVT simulations were performed subsequently for another 15 ns for equilibration followed by 20 ns of data production. The data were collected at every 10 fs from the last 5 ns of the NVT simulation which were then used to determine the structural and dynamic properties of the simulated kaolinite-PFAS model. Further details about the simulation methods and data analysis can be found in supporting information and in previous papers.[66,79,80]

Results and Discussion

Atomic Density Profiles

The atomic density profiles (ADPs) of PFAS, H_2O and metal cations as functions of the distance normal to the external (001) surface of kaolinite are shown in Figures 2a-2d, Figures S1a-S1d, Figures S2a-S2d and Figures S3a-S3d. The ADPs clearly indicate that irrespective of the cationic kaolinite models, all PFAS molecules are exclusively adsorbed on the hydroxyl surface while the cations are adsorbed near the siloxane surface which is in excellent agreement with

183 previous simulation studies on hydrated surfaces with polar molecules, namely citric acid.[54]
184 Importantly, the presence of deprotonated carboxylate and sulfonate functional groups closer to
185 the hydroxyl surface of kaolinite evidently demonstrates that the interaction of PFAS with the
186 surface is dictated by the direct coordination of the terminal functional groups (COO^-/SO_3^-) with
187 the hydroxyl surface and not through their hydrophobic carbon backbone. However, the ADPs
188 clearly illustrate that the interfacial adsorption structure varies significantly between carboxylate
189 and sulfonate PFAS molecules (Figure 2a-2d). For instance, the PFBA and PFOA molecules in
190 the simulated Ca-kaolinite model exhibit coordination with the hydroxyl surface through both the
191 'O' atoms of COO^- groups which is evident by the presence of equal intensity peaks at ~2.6 Å
192 from the surface (Figure 2a and 2c). In contrast, the coordination of PFBS and PFOS with the
193 hydroxyl surface is predominantly driven by only one 'O' atom of the SO_3^- groups and is
194 characterized by a distinct peak at ~2.0 Å (Figure 2b and 2d) while the other two 'O' atoms are
195 primarily located at larger distances (~4.1 Å) from the hydroxyl surface along with very small
196 peaks at ~2.0 Å. Such distributions clearly suggest that the probability of later two 'O' atoms of
197 SO_3^- groups coordinating with the hydroxyl surface is highly unlikely. In addition, the ADPs
198 clearly exhibit well-defined peaks for all the atoms of PFBS and PFOS in comparison to PFBA
199 and PFOA. For instance, the ADPs of C_{COO-} have two peaks centered at ~3.2 Å and ~4.9 Å along
200 with a broad distribution that extends up to 8 Å in contrast to only one peak for S_{SO3-} centered at
201 ~3.3 Å in sulfonate PFAS molecules.

202 Most importantly, irrespective of the terminal functional groups, the interfacial adsorption
203 structure is not influenced by the length of the PFAS molecules. The only difference observed is
204 that the ADPs extend further into the nanopore region along the surface normal for both PFOA
205 and PFOS (Figure 2c and 2d). This implies that the surface adsorbed PFAS molecules likely

206 protrude from the hydroxyl surface and do not prefer the hydrophobic part being parallel to the
207 surface (Figure 2a-2d). Furthermore, the metal cations do not show any influence on the interfacial
208 structure of any given PFAS molecules as the cations are exclusively adsorbed near the siloxane
209 surface (Figure S4 and S5). The ADPs of O_{H2O} at the hydroxyl surface exhibit three peaks at
210 distances ~2.6, 4.3, and 6.4 Å along with a broad distribution between ~8-10 Å and are in excellent
211 agreement with the ADPs of previous simulation studies of hydrated nanopores of kaolinite and
212 similar mineral, namely gibbsite.[80,81] Such agreements with kaolinite-H_2O simulations clearly
213 illustrate that the H_2O adsorption behavior is not influenced by the presence of short- and long-
214 chain PFAS molecules and their functionalities in the interfacial region. It is important to highlight
215 that the use of the M-O-H bending potential[61] allows the hydroxyl groups in kaolinite to probe
216 non-perpendicular orientation along the *z* dimension, thus enabling a prominent peak for H_{H2O} (~
217 1.7 Å) which potentially exhibits H-bonding interactions with the surface.

218 The ADPs of metal cations at the siloxane surface vary significantly depending upon their
219 charge densities and are not influenced by the presence of PFAS molecules at the hydroxyl surface
220 as shown in Figure S6a-S6f. The figures clearly indicate that both Ca^{2+} and Na^{+} ions are
221 predominantly adsorbed at distances 4.5 and 4.2 Å from the siloxane surface which represent outer
222 sphere coordination with respect to the surface. In contrast, K^{+} ions exhibit both inner- and outer-
223 sphere coordination with peaks at 2.9 and 4.9 Å from the siloxane surface, respectively.
224 Importantly, the ADPs of H_2O at the siloxane surface are almost identical irrespective of the metal
225 cations for all kaolinite models. The ADPs of O_{H2O} exhibit two distinct peaks centered at 2.7 and
226 6.2 Å along with a broad flat distribution between 3.3-4.8 Å from the siloxane surface, in excellent
227 agreement with previous studies on hydrated kaolinite models.[54,80] In addition, the well-defined
228 peaks for both O_{H2O} and H_{H2O} near the hydroxyl surface compared to those of the siloxane surface

229 are mostly likely due to the presence of strong H-bonding interactions (both donating and
230 accepting H-bonds) with the hydroxyl surface and is good agreement with the previous *ab initio*
231 MD studies of hydrated kaolinite.[82]

232 **Orientation of Surface-Adsorbed PFAS and H_2O**

233 It is imperative to calculate the orientation of PFAS molecules adsorbed on the hydroxyl
234 surface as the ADPs illustrate substantial differences between the terminal functional groups. The
235 orientations of surface adsorbed carboxylate and sulfonate PFAS with respect to the surface normal
236 were determined only for the molecules that represent the first peak for C_{COO-} ($z < 4.0$ Å) and S_{SO3-}
237 ($z < 4.1$ Å) in the ADPs for all kaolinite models. It is evident from Figure 3a that the surface
238 adsorbed PFBA and PFOA molecules in Ca-kaolinite have their COO^- groups oriented towards
239 the hydroxyl surface with an angle (θ_1) of ~125º and ~129º, respectively. In addition, the presence
240 of a second peak at high angles (θ_1 – ~160º) for PFOA denotes that the long-chain PFAS molecules
241 favor near-perpendicular orientation with respect to the hydroxyl surface compared to short-chain
242 PFAS. Importantly, the broad angular distribution in Figure 3a demonstrates that the surface-
243 adsorbed COO^- groups experience a rocking motion towards and away from the hydroxyl surface
244 of kaolinite (Figure S7). As for the ADPs, the orientational characteristics of PFBA and PFOA are
245 very similar between different cationic models with a slight variation of ±4º in the peak maxima
246 for θ_1 (Figures S8 and S9).

247 In contrast, the SO_3^- groups in PFBS and PFOS are predominantly oriented at an angle (θ_2) of
248 ~105º and ~100º, respectively with respect to the surface normal (Figure 3b). Although, the vector
249 is oriented marginally towards the hydroxyl surface, these θ_2 values indicate that the SO_3^- groups
250 in PFBS and PFOS molecules are oriented almost parallel to the hydroxyl surface. Such orientation
251 of SO_3^- groups shows that not all of the 'O' atoms are oriented perpendicular to the surface and is

in good correlation with only one 'O' peak of SO_3^- group being closer to the hydroxyl surface of kaolinite in the ADPs. Meanwhile, the presence of additional peaks at high angles (θ_2 > 130º) implies that the SO_3^- groups also exhibit a rocking motion towards and away from the hydroxyl surface (Figure 3b). However, the small peak intensities suggest that such reorientation of SO_3^- groups is substantially restricted in sulfonate molecules when compared to carboxylate PFAS molecules. Importantly, the overall orientational characteristics of PFBS and PFOS are not perturbed between kaolinite models with different metal cations except for a small redistribution of peaks for θ_2 angles that are greater than 130º, similar as for carboxylate PFAS molecules (Figure S8 and S9). In order to further confirm the interfacial structure of the SO_3^- group for surface adsorbed sulfonate PFAS molecules, the orientations of each S-O bond vector with respect to the surface normal for PFOS in different cationic kaolinite models were computed and are shown in Figure S10a-S10c. The distinct high angle peaks (θ_{SO1} - ~170º) for only one S-O_1 bond vector clearly validate that only the 'O' atoms of the SO_3^- groups are responsible for their coordination with the hydroxyl surface of kaolinite and agrees well with the ADP results.

Similar as for PFAS molecules, the orientations of the dipole vectors of adsorbed H_2O molecules with respect to the surface normal in Ca-kaolinite were calculated by considering only the molecules that belong to the first peak of O_{H2O} in ADPs for both the hydroxyl (z < 3.3 Å) and siloxane (z > 133.1 Å) surfaces. Figure 3c and Figure 3d clearly illustrate that the orientations of H_2O molecules are not influenced by the presence of PFAS molecules at the hydroxyl surface. Importantly, a distinct different in the orientation of the H_2O dipole is observed between the hydrophilic hydroxyl surface and hydrophobic siloxane surface. For instance, irrespective of the PFAS molecules, the dipole vectors of H_2O exhibit two different orientations with respect to the surface normal (Figure 3c). The θ_D value of ~20º represents H_2O dipoles that are oriented away

from the surface accepting H-bonds from the hydroxyl surface. The θ_D peak centered at ~127º represents H_2O dipoles oriented towards the hydroxyl surface and those H_2O molecules donates H-bonds to the surface. On the other hand, Figure 3d clearly indicates that the H_2O dipoles near the siloxane surface are oriented, on average, marginally towards the surface (θ_D - ~56º) which could be attributed to the hydrophobic character of the siloxane surface. The H_2O orientation near siloxane surface is in good agreement with recently reported contact angle (70º) studies of H_2O on similar hydrophobic siloxane surfaces of pyrophyllite.[83] In addition, it is evident from Figures 3, S8, and S9 that the H_2O orientations at both the hydroxyl and siloxane surfaces are almost identical between the different cationic kaolinite-PFAS models.

Adsorption Environment and Aggregation of PFAS

The adsorption environments of PFAS molecules at the hydroxyl surface of kaolinite are strongly influenced by the nature of the terminal functional groups and the length of the hydrophobic carbon backbone as demonstrated in Figures 4a-4d. It is highly evident from Figure 4a and 4c that both PFBA and PFOA exhibit direct coordination with the surface with only ~4-5 molecules, though all 16 of them are adsorbed at the interfacial region of the hydroxyl surface at any given time of the simulation. Importantly, the interfacial structure of PFBA and PFOA is completely contradictory to the complexation behavior of PFBS and PFOS where almost all molecules exhibit direct coordination with the hydroxyl surface (Figures 4b and 4d). Importantly, the presence of large number of surface coordinated sulfonate PFAS molecules when compared to carboxylate PFAS molecules is in excellent agreement with available experimental sorption isotherms, which report a higher adsorption of surface bound PFOS than of PFOA molecules in kaolinite at similar thermodynamic conditions.[43,46] Furthermore, Figures 4a-4d clearly illustrate that the surface adsorbed (~ 4-5) PFBA and PFOA molecules exhibit coordination with both of the

298 ‘O’ atoms of the COO^- group, while almost all PFBS and PFOS molecules explicitly demonstrate
299 that only one of the ‘O’ atoms of the SO_3^- group is coordinated to the hydroxyl surface. Such
300 adsorption environments for PFAS molecules with SO_3^- functional groups at the external (001)
301 surface of kaolinite are primarily responsible for the well-defined peaks in ADPs for PFBS and
302 PFOS rather than the carboxylate PFAS molecules (Figures 1a-1d). Similarly, the protrusion of
303 the surface adsorbed PFBS and PFOS from the hydroxyl surface is more prominent than with
304 PFBA and PFOA (Figure 4).

305 Most importantly, the simulations demonstrate that the aggregation behavior of PFAS varies
306 drastically between short- and long-chain molecules and significantly between different functional
307 groups having similar chain length (Figures 5a-5d). For instance, the PFBA and PFBS molecules
308 predominantly exist as monomers along with small, aggregated clusters which is completely
309 contradictory to the adsorption environment of PFOA and PFOS molecules that promote formation
310 of large, aggregated clusters varying in size and shape at the hydroxyl surfaces of kaolinite. For
311 instance, at the end of ~50 ns, four different cluster formation were observed for both PFOA and
312 PFOS molecules at the hydroxyl surface. Although the size of the aggregated clusters is very
313 similar between PFOA and PFOS, Figures 5c and 5d exhibit distinct differences in their
314 aggregation patterns. The PFOA aggregated cluster is comprised of a heptamer (4), a pentamer
315 (3), a trimer (1) and a monomer, where the values in the brackets represent the number of
316 molecules from each cluster exhibiting direct coordination with the hydroxyl surface of kaolinite.
317 The monomer, though near the surface, did not show any surface coordination. In contrast, the
318 aggregated cluster of PFOS consists of a hexamer (5), a pentamer (5), a trimer (3) along with two
319 surface bound monomers (Figures 4d and 5d). Thus, it is highly evident that almost all of the PFOS
320 molecules in the aggregated clusters exhibit direct coordination with the hydroxyl surface of

321 kaolinite in comparison to PFOA where only few molecules from each cluster establish surface
322 coordination. Importantly, the unique adsorption characteristics of PFOS could be one of the
323 critical factors responsible for showing high adsorption efficiency in kaolinite than PFOA in batch
324 sorption experiments.[45,46] Nevertheless, it should be highlighted that these aggregated clusters for
325 the long-chain PFAS molecules are formed as early as ~25 ns in the simulation and persist for the
326 remainder of the simulation run.

327 In contrast, when comparing the short-chain PFAS molecules, upon analyzing the trajectories,
328 the PFBA exist largely as monomers though a small number of dimers also form (Figure 5a). In
329 contrast, PFBS is dominantly present in dimer and trimer cluster configurations along with a few
330 monomers (Figure 5b). This indicates that the presence of the additional -CF_2- unit in PFBS
331 significantly favors the aggregation behavior. However, unlike the long-chain PFAS molecules,
332 the clusters in PFBA and PFBS are short-lived and constantly show association and dissociation
333 at random times which clearly suggests that the formation of thermodynamically stable aggregated
334 structures is highly improbable due to the short length of their hydrophobic backbones. Most
335 importantly, the simulations clearly portray that the non-bonded interactions between hydroxyl
336 surface atoms and the 'O' atoms of the PFAS (short- and long-chain) molecules plays a critical
337 role in determining the binding efficiency of PFAS in kaolinite at near neutral pH conditions. In
338 addition, the hydrophobic interactions between the PFAS molecules are pivotal for the formation
339 of large, aggregated clusters. This clearly underlines the importance of having a quantitative
340 evaluation of the individual energetic contributions to the surface complexation and aggregation
341 in future studies. The adsorption characteristics and aggregation behavior of all PFAS are very
342 similar between different cationic models and hence are presented in the supporting information
343 (Figure S11-S14).

The adsorption environments of PFAS, cations and H_2O were further validated by computing the radial distribution functions (RDF) and running coordination numbers (RCN) at both surfaces of Ca-kaolinite. It is evident from Figures 6a-6d, that the nearest neighbor coordination varies substantially between carboxylate and sulfonate PFAS molecules but is very similar for short- and long-chain PFAS that have the same functional groups. Irrespective of the length of the PFAS molecules, the mean interatomic distances for O_{COO^-} - H_{kaol} corresponds to 1.8 Å while for O_{SO3^-} - H_{kaol} the interatomic distance were centered at 1.7 Å. Although these values are similar between carboxylate and sulfonate PFAS molecules with 'H' atoms of the surface hydroxyls (H_{kaol}) in kaolinite, their RCN varies substantially. For instance, the nearest neighbor coordination of PFBA and PFOA is 0.5 suggesting that both of the 'O'_{COO-} atoms of the carboxylate group exhibit coordination with H_{kaol}. In contrast, the RCN of PFBS and PFOS with H_{kaol} atoms is 0.9 clearly demonstrates that only one 'O'_{SO3^-} atom of sulfonate is responsible for their coordination with the kaolinite hydroxyl surface which corroborates well with our structural interpretations. The mean 'O'_{COO^-} - O_{H2O} and 'O'_{SO3^-} - O_{H2O} interatomic distances are both centered at ~2.8 Å, similar to the values in bulk aqueous solution.[84,85] In addition, the comparable RCN values (2.9) for the 'O'_{COO^-} - O_{H2O} pair in studies on bulk solution further emphasize that not all carboxylate PFAS molecules are coordinated to the hydroxyl surface.[84] Importantly, due to the strong association of one 'O'_{SO3^-} atom with the hydroxyl surface, the RCN (1.3) with O_{H2O} is significantly lower compared to the value in previous studies of sulfonate ions in bulk solution.[85] Meanwhile, the analogous interatomic distances and RCN for the 'H'_{kaol} - O_{H2O} pair with all PFAS molecules evidently confirms our interpretation that the coordination of H_2O with the hydroxyl surface is not influenced by the presence of small and large aggregated PFAS molecules. Since the metal cations were

366 adsorbed at the siloxane surface, the coordination environments of PFAS with the hydroxyl surface
367 were similar for K- and Na-kaolinite models and hence not presented here.

368 The RDF and RCN of metal cations at the siloxane surface of kaolinite show that the
369 coordination environment is strongly correlated to the hydration properties of cations, irrespective
370 of type of PFAS molecule. For instance, Figure S15 illustrates that both Ca^{2+} and Na^{+} ions are
371 exclusively coordinated with eight and six H_2O molecules, and 0 O_b ('O' atoms at the tetrahedral
372 siloxane surface), representing outer sphere complexation. The reported RCN values of the metal
373 cations are in excellent agreement with those reported in previous studies both in bulk solutions
374 and in the mesopores of silicate minerals.[67,70] In contrast, K^{+} is coordinated by 6.7 H_2O molecules
375 and 0.5 O_b with a total RCN of 7.2, which is in excellent agreement with previous studies on bulk
376 solutions.[86] The low RCN with O_b implies the formation of weak inner sphere complexation of K^{+}
377 with the siloxane surface. As with the hydroxyl surface, the coordination structure of H_2O with O_b
378 is not influenced by the metal cations as evidenced by almost similar RCN values (0.5) for all
379 kaolinite models. It should be noted that the coordination environment is presented only for PFOS-
380 kaolinite models as the RDF and RCN of metal ions are highly identical with all PFAS models.

381 **Dynamics of PFAS**

382 The diffusion coefficients for all PFAS and H_2O molecules at the external (001) surface of
383 kaolinite were calculated using mean square displacements. It is evident from Table 1 that the
384 diffusion coefficients of all PFAS molecules (irrespective of length and functional groups) are
385 orders of magnitude smaller than the diffusion coefficient of H_2O. This restrictive dynamics of all
386 PFAS in different cationic kaolinite models stems from their adsorption at the hydroxyl surface of
387 kaolinite. Most importantly, the diffusion behavior of PFAS is strongly influenced both by the
388 nature of terminal functional group and the length of the hydrophobic component. For instance,

389 the diffusion coefficients of PFOA and PFOS are significantly lower than PFBA and PFBS
390 molecules, which could be attributed to the presence of surface adsorbed large, aggregated clusters
391 with long-chain PFAS. These decreasing diffusion characteristics with increasing molecular chain
392 length corroborates well with recently reported values using column experiments and diffusion
393 models on soils.[52] On the other hand, Table 1 clearly demonstrates that the diffusion coefficients
394 of sulfonate PFAS molecules are an order of magnitude smaller than the those of carboxylate,
395 which could be primarily attributed to the direct surface coordinated environments of PFBS and
396 PFOS. In contrast, since only few molecules of PFBA and PFOA exhibit direct coordination with
397 hydroxyl surface, their diffusion is relatively less restricted. Nevertheless, it should be emphasized
398 that the surface adsorbed PFAS molecules will exhibit restricted diffusion as compared to
399 molecules in the near surface region which will be examined in future studies.

400 It should be noted that the reported H_2O diffusion coefficient on the external surface of
401 kaolinite is not influenced by the presence of PFAS molecules and different cations. These values
402 are in excellent agreement with the computed self-diffusion coefficients of bulk SPC water.[63,66,69]
403 Since all of the values are similar for all models, Table 1 reports only on the kaolinite model with
404 PFOS molecules. However, it should be noted that the diffusion of H_2O molecules at the hydroxyl
405 surface of kaolinite will be substantially more restricted (due to H-bonding network) than at the
406 siloxane surface, as reported by earlier simulation studies on kaolinite.[66]

407 **Environmental Implications**

408 An in-depth understanding of the adsorption behavior of PFAS molecules in different clay
409 minerals is central to determining the fate and transport of PFAS in soils and sediments. The
410 current study is one of the first mechanistic study that provides a clear description about the critical
411 role of the hydroxyl surface in kaolinite in regulating the adsorption, interfacial structure and

412 dynamics of PFAS at natural conditions. Irrespective of the functional groups, the long-chain
413 PFAS molecules were strongly adsorbed at the hydroxyl surface forming highly localized large
414 aggregated admicellar type clusters. In contrast, the direct coordination PFBS with hydroxyl
415 surface suggest that the short-chain sulfonate PFAS molecules experiences more restrictive
416 transport in soils with high fraction of kaolinite when compared to carboxylate ones. Importantly,
417 the exclusive adsorption of short- and long-chain PFAS to the hydroxyl surface of kaolinite clearly
418 emphasizes the fact that most PFAS molecules in a contaminated soils could be associated at the
419 interparticle pore spaces of kaolinite particles and potentially other minerals with basal hydroxyl
420 groups, such as gibbsite. The absence of structural charge and surface charge compensating cations
421 in these minerals allows the complete basal hydroxyl surface accessible for all types of PFAS thus
422 resulting in high adsorption capacity in experiments.[43,45–47] In addition, although the current study
423 was performed with high concentration of PFAS that are representative of samples near U.S.
424 military installation sites, the results indicate that the interfacial adsorption structure and dynamics
425 would be very similar for contaminated samples with low concentration of PFAS. The only
426 difference could be on the size of the aggregated PFAS clusters which would vary depending on
427 the PFAS concentration.

428 Based on the excellent sorption and restrictive behavior of PFAS in kaolinite, it is important
429 to emphasize that kaolinite could be considered as a potential candidate for soil enrichment in the
430 context of immobilizing the long-chain PFAS and substantially hinder the transport of short-chain
431 PFAS molecules in near- and sub-surface regions, and, in groundwater regions. Furthermore, the
432 possibility of developing kaolinite based adsorbents should be further evaluated for eliminating
433 the PFAS molecules in surface and groundwaters. Importantly, this study will serve as basis for
434 evaluating the competitive interactions between PFAS molecules, and, with other organic matter

435 for adsorption at the interparticle pores of kaolinite surface. Such studies are highly warranted as
436 the contaminated samples contains a heterogeneous mixture of PFAS and soil organics.

437 **ACKNOWLEDGMENTS**

438 "This material is based upon work supported by the National Science Foundation under Grant no.
439 CHE-2107155." The authors gratefully appreciate this support. The authors also acknowledge
440 computational resources from the National Energy Research Scientific Computing Center, which
441 is supported by the Office of Science of the U.S. Department of Energy under ERCAP No. m1649
442 and the iCER computational facility at Michigan State University.

443 **ASSOCIATED CONTENT**

444 **Supporting Information:** Atomic density profiles, orientational and aggregation behavior of all
445 4 examined PFAS molecules with K- and Na-kaolinite systems. Rocking motion of PFOA at the
446 hydroxyl surface of Ca-kaolinite, coordination environments of metal cations with H_2O and basal
447 siloxane surface. Average cell dimensions of kaolinite at the end of NPT simulations. Additional
448 details about simulation techniques and analysis.

449 **Notes**

450 The authors declare no competing financial interest.

451

452

453

454

455

References

(1) Epa, U. S. EPA's Per- and Polyfluoroalkyl Substances (PFAS) Action Plan. **2019**, No. February.

(2) European Environment Agency. Emerging Chemical Risks in Europe-PFAS. **2019**, 1–15.

(3) Post, G. B. Recent US State and Federal Drinking Water Guidelines for Per- and Polyfluoroalkyl Substances. *Environ. Toxicol. Chem.* **2021**, *40* (3), 550–563. https://doi.org/10.1002/etc.4863.

(4) Zhang, X.; Lohmann, R.; Dassuncao, C.; Hu, X. C.; Weber, A. K.; Vecitis, C. D.; Sunderland, E. M. Source Attribution of Poly- and Perfluoroalkyl Substances (PFASs) in Surface Waters from Rhode Island and the New York Metropolitan Area. *Environ. Sci. Technol. Lett.* **2016**, *3* (9), 316–321. https://doi.org/10.1021/acs.estlett.6b00255.

(5) Del Vento, S.; Halsall, C.; Gioia, R.; Jones, K.; Dachs, J. Volatile Per- and Polyfluoroalkyl Compounds in the Remote Atmosphere of the Western Antarctic Peninsula: An Indirect Source of Perfluoroalkyl Acids to Antarctic Waters? *Atmos. Pollut. Res.* **2012**, *3* (4), 450–455. https://doi.org/10.5094/APR.2012.051.

(6) Krafft, M. P.; Riess, J. G. Per- and Polyfluorinated Substances (PFASs): Environmental Challenges. *Curr. Opin. Colloid Interface Sci.* **2015**, *20* (3), 192–212. https://doi.org/10.1016/j.cocis.2015.07.004.

(7) Foguth, R.; Sepúlveda, M. S.; Cannon, J. Per-and Polyfluoroalkyl Substances (PFAS) Neurotoxicity in Sentinel and Non-Traditional Laboratory Model Systems: Potential Utility in Predicting Adverse Outcomes in Human Health. *Toxics* **2020**, *8* (2), 1–20. https://doi.org/10.3390/TOXICS8020042.

(8) Sunderland, E. M.; Hu, X. C.; Dassuncao, C.; Tokranov, A. K.; Wagner, C. C.; Allen, J. G. A Review of the Pathways of Human Exposure to Poly- and Perfluoroalkyl Substances (PFASs) and Present Understanding of Health Effects. *J. Expo. Sci. Environ. Epidemiol.* **2019**, *29* (2), 131–147. https://doi.org/10.1038/s41370-018-0094-1.

(9) Buck, R. C.; Franklin, J.; Berger, U.; Conder, J. M.; Cousins, I. T.; Voogt, P. De; Jensen, A. A.; Kannan, K.; Mabury, S. A.; van Leeuwen, S. P. J. Perfluoroalkyl and Polyfluoroalkyl Substances in the Environment: Terminology, Classification, and Origins. *Integr. Environ. Assess. Manag.* **2011**, *7* (4), 513–541. https://doi.org/10.1002/ieam.258.

(10) Gagliano, E.; Sgroi, M.; Falciglia, P. P.; Vagliasindi, F. G. A.; Roccaro, P. Removal of Poly- and Perfluoroalkyl Substances (PFAS) from Water by Adsorption: Role of PFAS Chain Length, Effect of Organic Matter and Challenges in Adsorbent Regeneration. *Water Res.* **2020**, *171*, 115381. https://doi.org/10.1016/j.watres.2019.115381.

(11) Rappazzo, K. M.; Coffman, E.; Hines, E. P. Exposure to Perfluorinated Alkyl Substances and Health Outcomes in Children: A Systematic Review of the Epidemiologic Literature. *Int. J. Environ. Res. Public Health* **2017**, *14* (7), 1–22. https://doi.org/10.3390/ijerph14070691.

(12) Szilagyi, J. T.; Avula, V.; Fry, R. C. Perfluoroalkyl Substances (PFAS) and Their Effects on the Placenta, Pregnancy, and Child Development: A Potential Mechanistic Role for

Placental Peroxisome Proliferator–Activated Receptors (PPARs). *Curr. Environ. Heal. Reports* **2020**, *7* (3), 222–230. https://doi.org/10.1007/s40572-020-00279-0.

(13) Anderko, L.; Pennea, E. Exposures to Per-and Polyfluoroalkyl Substances (PFAS): Potential Risks to Reproductive and Children's Health. *Curr. Probl. Pediatr. Adolesc. Health Care* **2020**, *50* (2), 100760. https://doi.org/https://doi.org/10.1016/j.cppeds.2020.100760.

(14) Roth, J.; Abusallout, I.; Hill, T.; Holton, C.; Thapa, U.; Hanigan, D. Release of Volatile Per- and Polyfluoroalkyl Substances from Aqueous Film-Forming Foam. *Environ. Sci. Technol. Lett.* **2020**, *7* (3), 164–170. https://doi.org/10.1021/acs.estlett.0c00052.

(15) Xu, Y.; Jurkovic-Mlakar, S.; Li, Y.; Wahlberg, K.; Scott, K.; Pineda, D.; Lindh, C. H.; Jakobsson, K.; Engström, K. Association between Serum Concentrations of Perfluoroalkyl Substances (PFAS) and Expression of Serum MicroRNAs in a Cohort Highly Exposed to PFAS from Drinking Water. *Environ. Int.* **2020**, *136*, 105446. https://doi.org/https://doi.org/10.1016/j.envint.2019.105446.

(16) Hu, X. C.; Andrews, D. Q.; Lindstrom, A. B.; Bruton, T. A.; Schaider, L. A.; Grandjean, P.; Lohmann, R.; Carignan, C. C.; Blum, A.; Balan, S. A.; Higgins, C. P.; Sunderland, E. M. Detection of Poly- and Perfluoroalkyl Substances (PFASs) in U.S. Drinking Water Linked to Industrial Sites, Military Fire Training Areas, and Wastewater Treatment Plants. *Environ. Sci. Technol. Lett.* **2016**, *3* (10), 344–350. https://doi.org/10.1021/acs.estlett.6b00260.

(17) Lai, T. T.; Eken, Y.; Wilson, A. K. Binding of Per- and Polyfluoroalkyl Substances to the Human Pregnane X Receptor. *Environ. Sci. Technol.* **2020**, *54* (24), 15986–15995. https://doi.org/10.1021/acs.est.0c04651.

(18) Almeida, N. M. S.; Eken, Y.; Wilson, A. K. Binding of Per- and Polyfluoro-Alkyl Substances to Peroxisome Proliferator-Activated Receptor Gamma. *ACS Omega* **2021**, *6* (23), 15103–15114. https://doi.org/10.1021/acsomega.1c01304.

(19) Ahrens, L.; Bundschuh, M. Fate and Effects of Poly- and Perfluoroalkyl Substances in the Aquatic Environment: A Review. *Environ. Toxicol. Chem.* **2014**, *33* (9), 1921–1929. https://doi.org/10.1002/etc.2663.

(20) Ahrens, L. Polyfluoroalkyl Compounds in the Aquatic Environment: A Review of Their Occurrence and Fate. *J. Environ. Monit.* **2011**, *13* (1), 20–31. https://doi.org/10.1039/c0em00373e.

(21) Wei, C.; Song, X.; Wang, Q.; Hu, Z. Sorption Kinetics, Isotherms and Mechanisms of PFOS on Soils with Different Physicochemical Properties. *Ecotoxicol. Environ. Saf.* **2017**, *142* (March), 40–50. https://doi.org/10.1016/j.ecoenv.2017.03.040.

(22) Munoz, G.; Labadie, P.; Botta, F.; Lestremau, F.; Lopez, B.; Geneste, E.; Pardon, P.; Dévier, M. H.; Budzinski, H. Occurrence Survey and Spatial Distribution of Perfluoroalkyl and Polyfluoroalkyl Surfactants in Groundwater, Surface Water, and Sediments from Tropical Environments. *Sci. Total Environ.* **2017**, *607–608*, 243–252. https://doi.org/10.1016/j.scitotenv.2017.06.146.

(23) Lampert, D. J. Emerging Research Needs for Assessment and Remediation of Sediments Contaminated with Per- and Poly-Fluoroalkyl Substances. *Curr. Pollut. Reports* **2018**, *4*

(4), 277–279. https://doi.org/10.1007/s40726-018-0098-4.

(24) Milinovic, J.; Lacorte, S.; Vidal, M.; Rigol, A. Sorption Behaviour of Perfluoroalkyl Substances in Soils. *Sci. Total Environ.* **2015**, *511*, 63–71. https://doi.org/10.1016/j.scitotenv.2014.12.017.

(25) Xiao, F.; Jin, B.; Golovko, S. A.; Golovko, M. Y.; Xing, B. Sorption and Desorption Mechanisms of Cationic and Zwitterionic Per- And Polyfluoroalkyl Substances in Natural Soils: Thermodynamics and Hysteresis. *Environ. Sci. Technol.* **2019**, *53* (20), 11818–11827. https://doi.org/10.1021/acs.est.9b05379.

(26) Fabregat-Palau, J.; Vidal, M.; Rigol, A. Modelling the Sorption Behaviour of Perfluoroalkyl Carboxylates and Perfluoroalkane Sulfonates in Soils. *Sci. Total Environ.* **2021**, *801*. https://doi.org/10.1016/j.scitotenv.2021.149343.

(27) Brusseau, M. L.; Anderson, R. H.; Guo, B. PFAS Concentrations in Soils: Background Levels versus Contaminated Sites. *Sci. Total Environ.* **2020**, *740*, 140017. https://doi.org/10.1016/j.scitotenv.2020.140017.

(28) Li, F.; Fang, X.; Zhou, Z.; Liao, X.; Zou, J.; Yuan, B.; Sun, W. Adsorption of Perfluorinated Acids onto Soils: Kinetics, Isotherms, and Influences of Soil Properties. *Sci. Total Environ.* **2019**, *649*, 504–514. https://doi.org/10.1016/j.scitotenv.2018.08.209.

(29) Nguyen, T. M. H.; Bräunig, J.; Thompson, K.; Thompson, J.; Kabiri, S.; Navarro, D. A.; Kookana, R. S.; Grimison, C.; Barnes, C. M.; Higgins, C. P.; Mclaughlin, M. J.; Mueller, J. F. Influences of Chemical Properties, Soil Properties, and Solution PH on Soil-Water Partitioning Coefficients of Per- And Polyfluoroalkyl Substances (PFASs). *Environ. Sci. Technol.* **2020**, *54* (24), 15883–15892. https://doi.org/10.1021/acs.est.0c05705.

(30) Ross, I.; McDonough, J.; Miles, J.; Storch, P.; Thelakkat Kochunarayanan, P.; Kalve, E.; Hurst, J.; S. Dasgupta, S.; Burdick, J. A Review of Emerging Technologies for Remediation of PFASs. *Remediation* **2018**, *28* (2), 101–126. https://doi.org/10.1002/rem.21553.

(31) Duchesne, A. L.; Brown, J. K.; Patch, D. J.; Major, D.; Weber, K. P.; Gerhard, J. I. Remediation of PFAS-Contaminated Soil and Granular Activated Carbon by Smoldering Combustion. *Environ. Sci. Technol.* **2020**, *54* (19), 12631–12640. https://doi.org/10.1021/acs.est.0c03058.

(32) Maimaiti, A.; Deng, S.; Meng, P.; Wang, W.; Wang, B.; Huang, J.; Wang, Y.; Yu, G. Competitive Adsorption of Perfluoroalkyl Substances on Anion Exchange Resins in Simulated AFFF-Impacted Groundwater. *Chem. Eng. J.* **2018**, *348* (February), 494–502. https://doi.org/10.1016/j.cej.2018.05.006.

(33) Johnson, J. K.; Hoffman, C. M.; Smith, D. A.; Xia, Z. Advanced Filtration Membranes for the Removal of Perfluoroalkyl Species from Water. *ACS Omega* **2019**, *4* (5), 8001–8006. https://doi.org/10.1021/acsomega.9b00314.

(34) Mahinroosta, R.; Senevirathna, L. A Review of the Emerging Treatment Technologies for PFAS Contaminated Soils. *J. Environ. Manage.* **2020**, *255* (June 2019), 109896. https://doi.org/10.1016/j.jenvman.2019.109896.

(35) Sorengard, M.; Kleja, D. B.; Ahrens, L. Stabilization of Per- and Polyfluoroalkyl Substances (PFASs) with Colloidal Activated Carbon (PlumeStop®) as a Function of Soil Clay and

Organic Matter Content. *J. Environ. Manage.* **2019**, *249* (May), 109345. https://doi.org/10.1016/j.jenvman.2019.109345.

(36) Shi, Y.; Sun, Y.; Gao, B.; Xu, H.; Wu, J. Importance of Organic Matter to the Retention and Transport of Bisphenol A and Bisphenol S in Saturated Soils. *Water. Air. Soil Pollut.* **2019**, *230* (2), 1–9. https://doi.org/10.1007/s11270-019-4096-y.

(37) Lee, S. S.; Nagy, K. L.; Park, C.; Fenter, P. Heavy Metal Sorption at the Muscovite (001)–Fulvic Acid Interface. *Environ. Sci. Technol.* **2011**, *45* (22), 9574–9581. https://doi.org/10.1021/es201323a.

(38) Sposito, G. *The Chemistry of Soils*, 2nd ed.; Oxford University Press: New York, 2008; p. 329.

(39) Loganathan, N.; Yazaydin, A. O.; Bowers, G. M.; Kalinichev, A. G.; Kirkpatrick, R. J. Molecular Dynamics Study of CO2 and H2O Intercalation in Smectite Clays: Effect of Temperature and Pressure on Interlayer Structure and Dynamics in Hectorite. *J. Phys. Chem. C* **2017**, *121* (39), 24527–24540. https://doi.org/10.1021/acs.jpcc.7b06825.

(40) Lee, S. S.; Nagy, K. L.; Park, C.; Fenter, P. Enhanced Uptake and Modified Distribution of Mercury(II) by Fulvic Acid on the Muscovite (001) Surface. *Environ. Sci. Technol.* **2009**, *43* (14), 5295–5300. https://doi.org/10.1021/es900214e.

(41) Bertsch, P. M.; Seaman, J. C. Characterization of Complex Mineral Assemblages: Implications for Contaminant Transport and Environmental Remediation. *Proc. Natl. Acad. Sci.* **1999**, *96* (7), 3350 LP – 3357. https://doi.org/10.1073/pnas.96.7.3350.

(42) Petrović, M.; Kaštelan-macan, M.; Horvat, A. J. M. Interactive Sorption of Metal Ions and Humic Acids onto Mineral Particles. *Water. Air. Soil Pollut.* **1999**, *111* (1), 41–56. https://doi.org/10.1023/A:1005084802830.

(43) Xiao, F.; Zhang, X.; Penn, L.; Gulliver, J. S.; Simcik, M. F. Effects of Monovalent Cations on the Competitive Adsorption of Perfluoroalkyl Acids by Kaolinite: Experimental Studies and Modeling. *Environ. Sci. Technol.* **2011**, *45* (23), 10028–10035. https://doi.org/10.1021/es202524y.

(44) Du, Z.; Deng, S.; Bei, Y.; Huang, Q.; Wang, B.; Huang, J.; Yu, G. Adsorption Behavior and Mechanism of Perfluorinated Compounds on Various Adsorbents-A Review. *J. Hazard. Mater.* **2014**, *274*, 443–454. https://doi.org/10.1016/j.jhazmat.2014.04.038.

(45) Jeon, J.; Kannan, K.; Lim, B. J.; An, K. G.; Kim, S. D. Effects of Salinity and Organic Matter on the Partitioning of Perfluoroalkyl Acid (PFAs) to Clay Particles. *J. Environ. Monit.* **2011**, *13* (6), 1803–1810. https://doi.org/10.1039/c0em00791a.

(46) Zhang, D. Q.; Zhang, W. L.; Liang, Y. N. Adsorption of Perfluoroalkyl and Polyfluoroalkyl Substances (PFASs) from Aqueous Solution - A Review. *Sci. Total Environ.* **2019**, *694*. https://doi.org/10.1016/j.scitotenv.2019.133606.

(47) Zhao, L.; Bian, J.; Zhang, Y.; Zhu, L.; Liu, Z. Comparison of the Sorption Behaviors and Mechanisms of Perfluorosulfonates and Perfluorocarboxylic Acids on Three Kinds of Clay Minerals. *Chemosphere* **2014**, *114* (May 2009), 51–58. https://doi.org/10.1016/j.chemosphere.2014.03.098.

(48) Higgins, C. P.; Luthy, R. G. Sorption of Perfluorinated Surfactants on Sediments. *Environ.*

Sci. Technol. **2006**, *40* (23), 7251–7256. https://doi.org/10.1021/es061000n.

(49) Zhang, R.; Yan, W.; Jing, C. Mechanistic Study of PFOS Adsorption on Kaolinite and Montmorillonite. *Colloids Surfaces A Physicochem. Eng. Asp.* **2014**, *462*, 252–258. https://doi.org/10.1016/j.colsurfa.2014.09.019.

(50) Mukhopadhyay, R.; Sarkar, B.; Palansooriya, K. N.; Dar, J. Y.; Bolan, N. S.; Parikh, S. J.; Sonne, C.; Ok, Y. S. Natural and Engineered Clays and Clay Minerals for the Removal of Poly- and Perfluoroalkyl Substances from Water: State-of-the-Art and Future Perspectives. *Adv. Colloid Interface Sci.* **2021**, *297* (September), 102537. https://doi.org/10.1016/j.cis.2021.102537.

(51) Brusseau, M. L. Simulating PFAS Transport Influenced by Rate-Limited Multi-Process Retention. *Water Res.* **2020**, *168*, 115179. https://doi.org/10.1016/j.watres.2019.115179.

(52) Schaefer, C. E.; Drennan, D.; Nickerson, A.; Maizel, A.; Higgins, C. P. Diffusion of Perfluoroalkyl Acids through Clay-Rich Soil. *J. Contam. Hydrol.* **2021**, *241* (November 2020), 103814. https://doi.org/10.1016/j.jconhyd.2021.103814.

(53) Willemsen, J. A. R.; Bourg, I. C. Molecular Dynamics Simulation of the Adsorption of Per- and Polyfluoroalkyl Substances (PFASs) on Smectite Clay. *J. Colloid Interface Sci.* **2021**, *585*, 337–346. https://doi.org/https://doi.org/10.1016/j.jcis.2020.11.071.

(54) Papavasileiou, K. D.; Michalis, V. K.; Peristeras, L. D.; Vasileiadis, M.; Striolo, A.; Economou, I. G. Molecular Dynamics Simulation of Water-Based Fracturing Fluids in Kaolinite Slit Pores. *J. Phys. Chem. C* **2018**, *122* (30), 17170–17183. https://doi.org/10.1021/acs.jpcc.8b03552.

(55) Greathouse, J. A.; Cygan, R. T.; Fredrich, J. T.; Jerauld, G. R. Adsorption of Aqueous Crude Oil Components on the Basal Surfaces of Clay Minerals: Molecular Simulations Including Salinity and Temperature Effects. *J. Phys. Chem. C* **2017**, *121* (41), 22773–22786. https://doi.org/10.1021/acs.jpcc.7b06454.

(56) Cygan, R. T.; Liang, J.-J.; Kalinichev, A. G. Molecular Models of Hydroxide, Oxyhydroxide, and Clay Phases and the Development of a General Force Field. *J. Phys. Chem. B* **2004**, *108* (4), 1255–1266. https://doi.org/10.1021/jp0363287.

(57) Plimpton, S. Fast Parallel Algorithms for Short-Range Molecular Dynamics. *J. Comput. Phys.* **1995**, *117* (1), 1–19. https://doi.org/https://doi.org/10.1006/jcph.1995.1039.

(58) Shinoda, W.; Shiga, M.; Mikami, M. Rapid Estimation of Elastic Constants by Molecular Dynamics Simulation under Constant Stress. *Phys. Rev. B* **2004**, *69* (13), 134103. https://doi.org/10.1103/PhysRevB.69.134103.

(59) Tuckerman, M. E.; Alejandre, J.; López-Rendón, R.; Jochim, A. L.; Martyna, G. J. A Liouville-Operator Derived Measure-Preserving Integrator for Molecular Dynamics Simulations in the Isothermal–Isobaric Ensemble. *J. Phys. A. Math. Gen.* **2006**, *39* (19), 5629–5651. https://doi.org/10.1088/0305-4470/39/19/s18.

(60) Plimpton, S.; Pollock, R.; Stevens, M. J. Particle Mesh Ewald and RRESPA for Parallel Molecular Dynamics Simulations. *Proc. Eighth Siam Conf. Parallel Process. Sci. Comput.* **1997**, 1–13.

(61) Pouvreau, M.; Greathouse, J. A.; Cygan, R. T.; Kalinichev, A. G. Structure of Hydrated

Kaolinite Edge Surfaces: DFT Results and Further Development of the ClayFF Classical Force Field with Metal-O-H Angle Bending Terms. *J. Phys. Chem. C* **2019**, *123* (18), 11628–11638. https://doi.org/10.1021/acs.jpcc.9b00514.

(62) Pouvreau, M.; Greathouse, J. A.; Cygan, R. T.; Kalinichev, A. G. Structure of Hydrated Gibbsite and Brucite Edge Surfaces: DFT Results and Further Development of the ClayFF Classical Force Field with Metal-O-H Angle Bending Terms. *J. Phys. Chem. C* **2017**, *121* (27), 14757–14771. https://doi.org/10.1021/acs.jpcc.7b05362.

(63) Teleman, O.; Jönsson, B.; Engström, S. A Molecular Dynamics Simulation of a Water Model with Intramolecular Degrees of Freedom. *Mol. Phys.* **1987**, *60* (1), 193–203. https://doi.org/10.1080/00268978700100141.

(64) Wang, J.; Wolf, R. M.; Caldwell, J. W.; Kollman, P. A.; Case, D. A. Development and Testing of a General Amber Force Field. *J. Comput. Chem.* **2004**, *25* (9), 1157–1174. https://doi.org/10.1002/jcc.20035.

(65) Cornell, W. D.; Cieplak, P.; Bayly, C. I.; Gould, I. R.; Merz, K. M.; Ferguson, D. M.; Spellmeyer, D. C.; Fox, T.; Caldwell, J. W.; Kollman, P. A. A Second Generation Force Field for the Simulation of Proteins, Nucleic Acids, and Organic Molecules. *J. Am. Chem. Soc.* **1995**, *117* (19), 5179–5197. https://doi.org/10.1021/ja00124a002.

(66) Loganathan, N.; Yazaydin, A. O.; Bowers, G. M.; Kalinichev, A. G.; Kirkpatrick, R. J. Structure, Energetics, and Dynamics of Cs+ and H2O in Hectorite: Molecular Dynamics Simulations with an Unconstrained Substrate Surface. *J. Phys. Chem. C* **2016**, *120* (19), 10298–10310. https://doi.org/10.1021/acs.jpcc.6b01016.

(67) Nanda, R.; Bowers, G. M.; Loganathan, N.; Burton, S. D.; Kirkpatrick, R. J. Temperature Dependent Structure and Dynamics in Smectite Interlayers: 23Na MAS NMR Spectroscopy of Na-Hectorite. *RSC Adv.* **2019**, *9* (22), 12755–12765. https://doi.org/10.1039/C9RA01056D.

(68) Loganathan, N.; Yazaydin, A. O.; Bowers, G. M.; Kalinichev, A. G.; Kirkpatrick, R. J. Cation and Water Structure, Dynamics, and Energetics in Smectite Clays: A Molecular Dynamics Study of Ca-Hectorite. *J. Phys. Chem. C* **2016**, *120* (23), 12429–12439. https://doi.org/10.1021/acs.jpcc.6b00230.

(69) Greathouse, J. A.; Hart, D. B.; Bowers, G. M.; Kirkpatrick, R. J.; Cygan, R. T. Molecular Simulation of Structure and Diffusion at Smectite–Water Interfaces: Using Expanded Clay Interlayers as Model Nanopores. *J. Phys. Chem. C* **2015**, *119* (30), 17126–17136. https://doi.org/10.1021/acs.jpcc.5b03314.

(70) Loganathan, N.; James Kirkpatrick, R.; Bowers, G. M. A Mechanistic Exploration of Natural Organic Matter Aggregation and Surface Complexation in Smectite Mesopores. *J. Phys. Chem. A* **2020**, *124* (47), 9832–9843.

(71) Kalinichev, A. G.; Loganathan, N.; Wakou, B. F. N.; Chen, Z. Interaction of Ions with Hydrated Clay Surfaces: Computational Molecular Modeling for Nuclear Waste Disposal Applications. *Procedia Earth Planet. Sci.* **2017**, *17*, 566–569. https://doi.org/10.1016/j.proeps.2016.12.144.

(72) Iskrenova-Tchoukova, E.; Kalinichev, A. G.; Kirkpatrick, R. J. Metal Cation Complexation with Natural Organic Matter in Aqueous Solutions: Molecular Dynamics Simulations and

Potentials of Mean Force. *Langmuir* **2010**, *26* (20), 15909–15919. https://doi.org/10.1021/la102535n.

(73) Bowers, G. M.; Singer, J. W.; Bish, D. L.; Kirkpatrick, R. J. Structural and Dynamical Relationships of Ca2+and H2O in Smectite/2H2O Systems. *Am. Mineral.* **2014**, *99* (2–3), 318–331. https://doi.org/10.2138/am.2014.4499.

(74) Bowers, G. M.; Argersinger, H. E.; Reddy, U. V.; Johnson, T. A.; Arey, B.; Bowden, M.; Kirkpatrick, R. J. Integrated Molecular and Microscopic Scale Insight into Morphology and Ion Dynamics in Ca2+-Mediated Natural Organic Matter Floccs. *J. Phys. Chem. C* **2015**, *119* (31), 17773–17783. https://doi.org/10.1021/acs.jpcc.5b05509.

(75) Reddy, U. V.; Bowers, G. M.; Loganathan, N.; Bowden, M.; Yazaydin, A. O.; Kirkpatrick, R. J. Water Structure and Dynamics in Smectites: X-Ray Diffraction and 2H NMR Spectroscopy of Mg–, Ca–, Sr–, Na–, Cs–, and Pb–Hectorite. *J. Phys. Chem. C* **2016**, *120* (16), 8863–8876. https://doi.org/10.1021/acs.jpcc.6b03431.

(76) Schaef, H. T.; Loganathan, N.; Bowers, G. M.; Kirkpatrick, R. J.; Yazaydin, A. O.; Burton, S. D.; Hoyt, D. W.; Thanthiriwatte, K. S.; Dixon, D. A.; McGrail, B. P.; Rosso, K. M.; Ilton, E. S.; Loring, J. S. Tipping Point for Expansion of Layered Aluminosilicates in Weakly Polar Solvents: Supercritical CO2. *ACS Appl. Mater. Interfaces* **2017**, *9* (42), 36783–36791. https://doi.org/10.1021/acsami.7b10590.

(77) Jakalian, A.; Bush, B. L.; Jack, D. B.; Bayly, C. I. Fast, Efficient Generation of High-Quality Atomic Charges. AM1-BCC Model: I. Method. *J. Comput. Chem.* **2000**, *21* (2), 132–146. https://doi.org/10.1002/(SICI)1096-987X(20000130)21:2<132::AID-JCC5>3.0.CO;2-P.

(78) Wang, J.; Wang, W.; Kollman, P. A.; Case, D. A. Automatic Atom Type and Bond Type Perception in Molecular Mechanical Calculations. *J. Mol. Graph. Model.* **2006**, *25* (2), 247–260. https://doi.org/https://doi.org/10.1016/j.jmgm.2005.12.005.

(79) Morrow, C. P.; Yazaydin, A. Ö.; Krishnan, M.; Bowers, G. M.; Kalinichev, A. G.; Kirkpatrick, R. J. Structure, Energetics, and Dynamics of Smectite Clay Interlayer Hydration: Molecular Dynamics and Metadynamics Investigation of Na-Hectorite. *J. Phys. Chem. C* **2013**, *117* (10), 5172–5187. https://doi.org/10.1021/jp312286g.

(80) Vasconcelos, I. F.; Bunker, B. A.; Cygan, R. T. Molecular Dynamics Modeling of Ion Adsorption to the Basal Surfaces of Kaolinite. *J. Phys. Chem. C* **2007**, *111* (18), 6753–6762. https://doi.org/10.1021/jp065687+.

(81) Wang, J.; Kalinichev, A. G.; Kirkpatrick, R. J. Effects of Substrate Structure and Composition on the Structure, Dynamics, and Energetics of Water at Mineral Surfaces: A Molecular Dynamics Modeling Study. *Geochim. Cosmochim. Acta* **2006**, *70* (3), 562–582. https://doi.org/10.1016/j.gca.2005.10.006.

(82) Tunega, D.; Gerzabek, M. H.; Lischka, H. Ab Initio Molecular Dynamics Study of a Monomolecular Water Layer on Octahedral and Tetrahedral Kaolinite Surfaces. *J. Phys. Chem. B* **2004**, *108* (19), 5930–5936. https://doi.org/10.1021/jp037121g.

(83) Miller, J. D.; Wang, X.; Jin, J.; Shrimali, K. Interfacial Water Structure and the Wetting of Mineral Surfaces. *Int. J. Miner. Process.* **2016**, *156*, 62–68. https://doi.org/10.1016/j.minpro.2016.02.004.

(84) Alagona, G.; Ghio, C.; Kollman, P. Monte Carlo Simulation Studies of the Solvation of Ions. 1. Acetate Anion and Methylammonium Cation. *J. Am. Chem. Soc.* **1986**, *108* (2), 185–191.

(85) Vchirawongkwin, V.; Pornpiganon, C.; Kritayakornupong, C.; Tongraar, A.; Rode, B. M. The Stability of Bisulfite and Sulfonate Ions in Aqueous Solution Characterized by Hydration Structure and Dynamics. *J. Phys. Chem. B* **2012**, *116* (37), 11498–11507. https://doi.org/10.1021/jp305648e.

(86) Koneshan, S.; Rasaiah, J. C.; Lynden-Bell, R. M.; Lee, S. H. Solvent Structure, Dynamics, and Ion Mobility in Aqueous Solutions at 25 °C. *J. Phys. Chem. B* **1998**, *102* (21), 4193–4204. https://doi.org/10.1021/jp980642x.

Figures

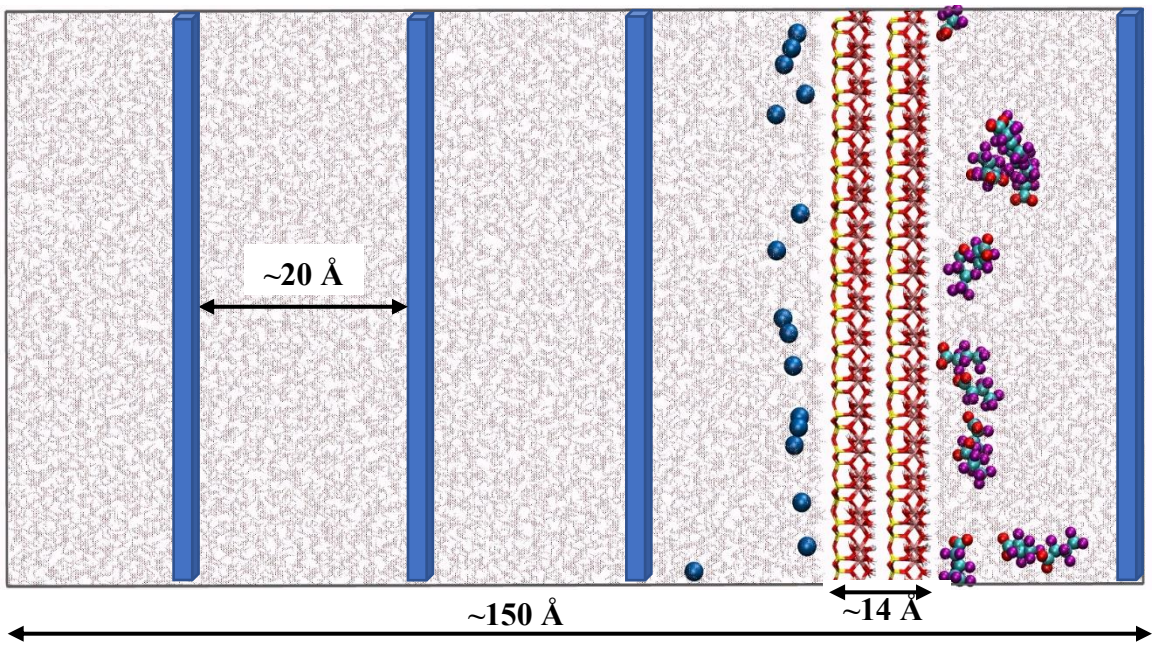

Figure 1: Pictorial representation of the simulated PFAS – kaolinite models. The rectangular blocks represent the initial position of the PFAS molecules at *t*=0 ns. Color codes: yellow sticks - Si tetrahedra; pink sticks – Al octahedral; red sticks – surface O; white sticks – hydroxyl H; blue spheres – cations; cyan spheres – C; purple spheres – F; red sphere – O (PFAS). H_2O molecules are shown as grayed stick representation.

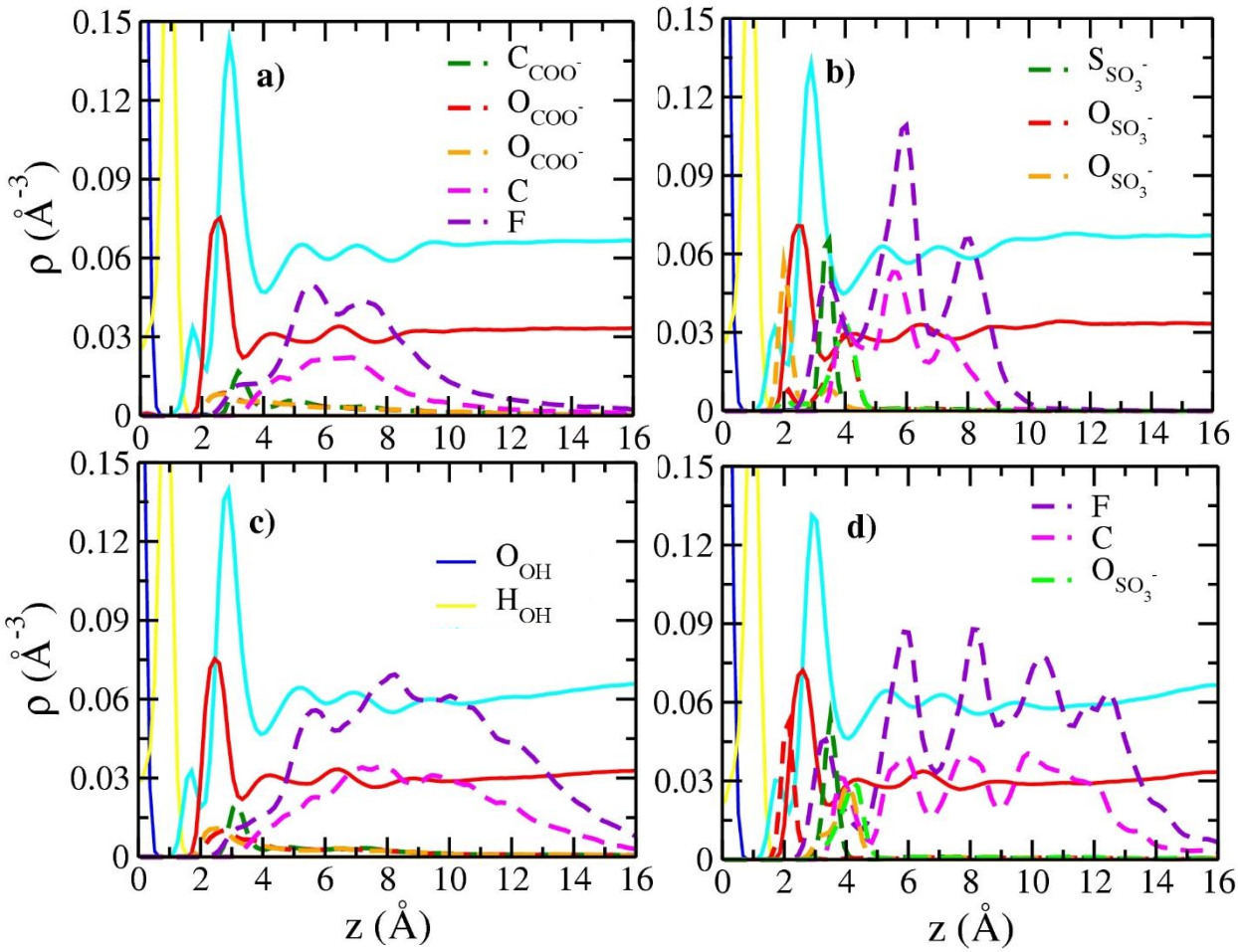

Figure 2: Computed atomic density profiles (ADPs) of PFAS and H_2O molecules in Ca-kaolinite as functions of distance from the external (001) hydroxyl surface for a) PFBA, b) PFBS, c) PFOA and d) PFOS. H_{OH} (solid yellow) and O_{OH} (solid blue) represents the hydrogens and oxygens of the hydroxyl groups in kaolinite, respectively. The O_{H2O} and H_{H2O} are shown as solid red and cyan. Dashed lines represent the atoms of PFAS molecule. z = 0 is the mean position of the basal O atoms at the hydroxyl surface of kaolinite.

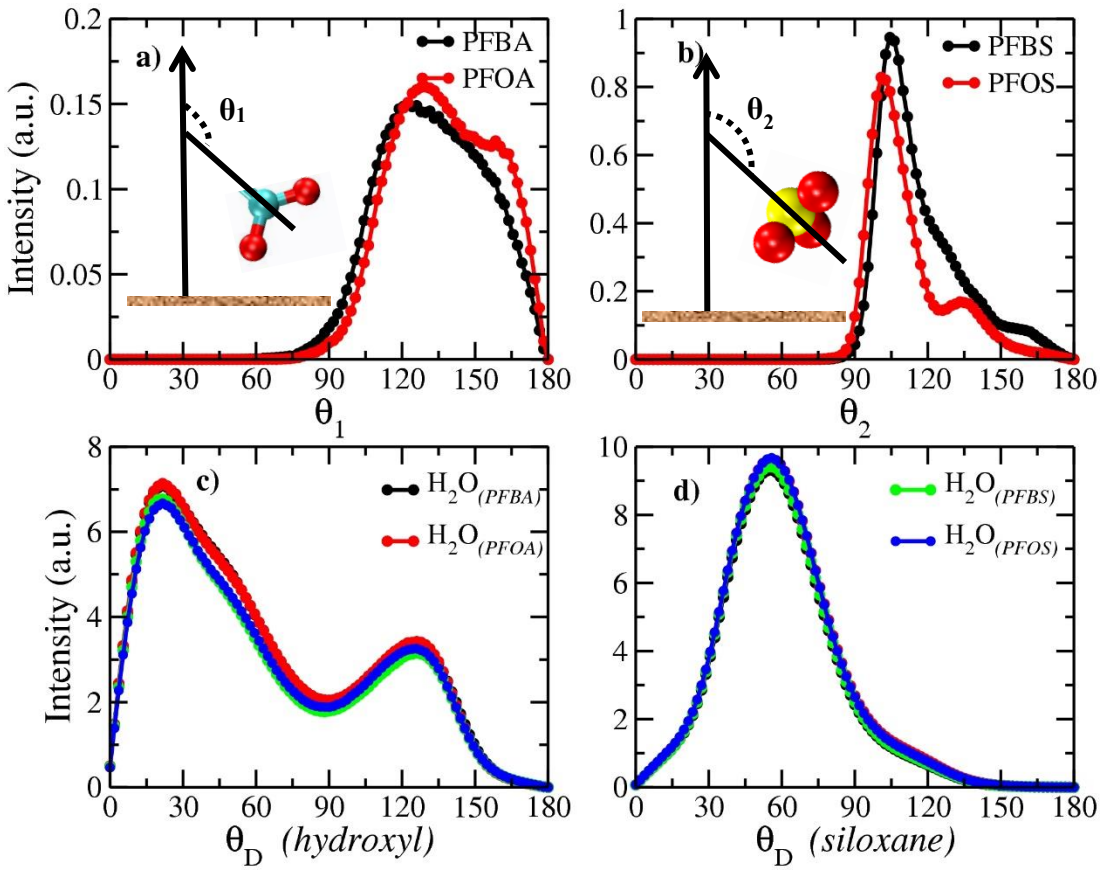

Figure 3: Computed orientation distributions of surface adsorbed PFAS molecules and H_2O dipoles at the external (001) surfaces of Ca-kaolinite. a) and b) represents orientation of PFAS molecules with respect to the hydroxyl surface; c) and d) represents orientations of dipole vector of H_2O (1st ADP peak) at the hydroxyl and siloxane surface. θ_1 is the angle between the vector bisecting the COO^- groups and the normal to the hydroxyl surface of kaolinite. θ_2 is the angle between the vector bisecting the SO_3^- groups and the normal to the hydroxyl surface of kaolinite. θ_D is the angle between the dipole vector of H_2O molecules and the normal to the hydroxyl/siloxane surface of kaolinite.

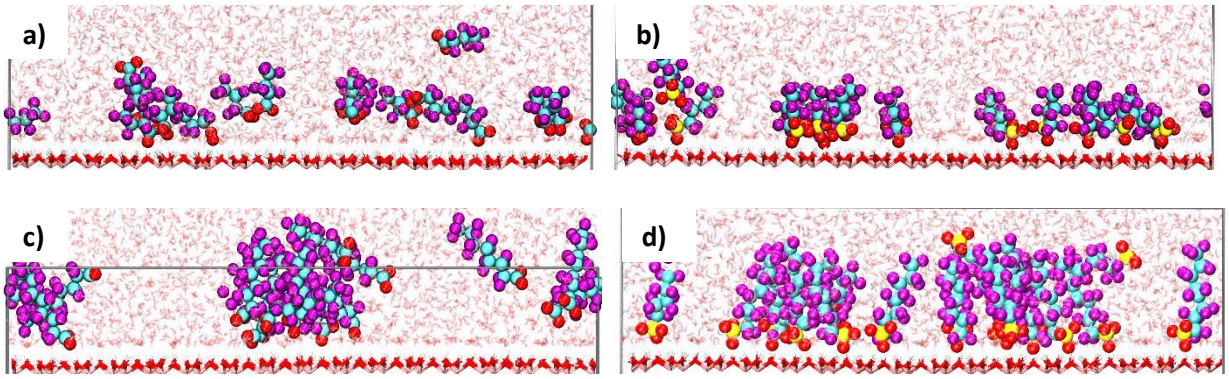

Figure 4: Pictorial representation of PFAS molecules at the interfacial region of external (001) hydroxyl surface of Ca-kaolinite. a) PFBA, b) PFBS, c) PFOA, d) PFOS. Color codes: pink sticks – Al octahedra; red sticks – hydroxyl O; white sticks – hydroxyl H; cyan spheres – C; purple spheres – F; red sphere – O (PFAS); yellow sphere – S. H_2O molecules are shown as grayed stick representation.

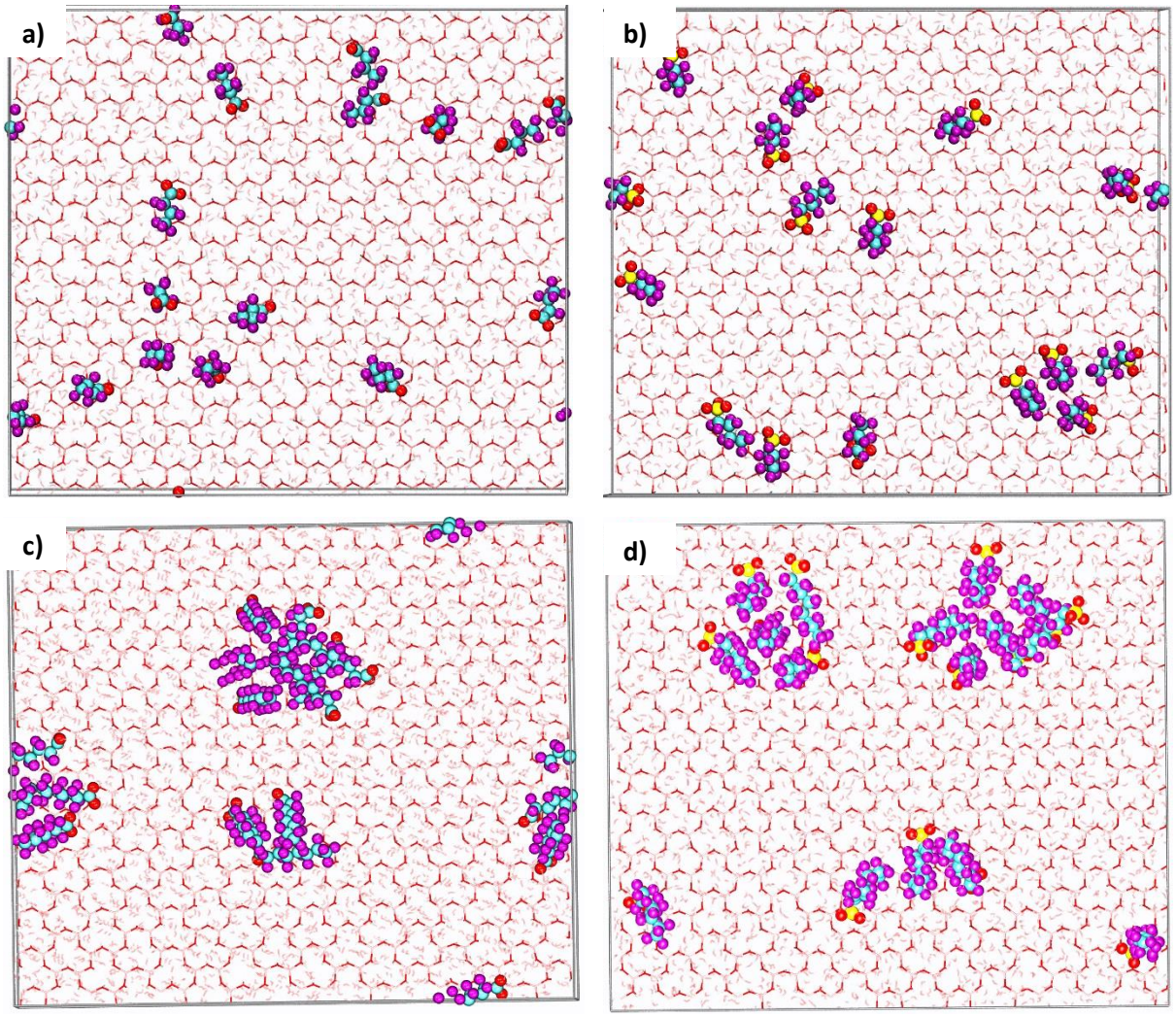

Figure 5: Pictorial representation of PFAS molecules at the external (001) hydroxyl surface of Ca-kaolinite. a) PFBA, b) PFBS, c) PFOA, d) PFOS. Color codes: pink sticks – Al octahedra; red sticks – hydroxyl O; white sticks – hydroxyl H; cyan spheres – C; purple spheres – F; red sphere – O (PFAS); yellow sphere – S. H_2O molecules are shown as grayed stick representation.

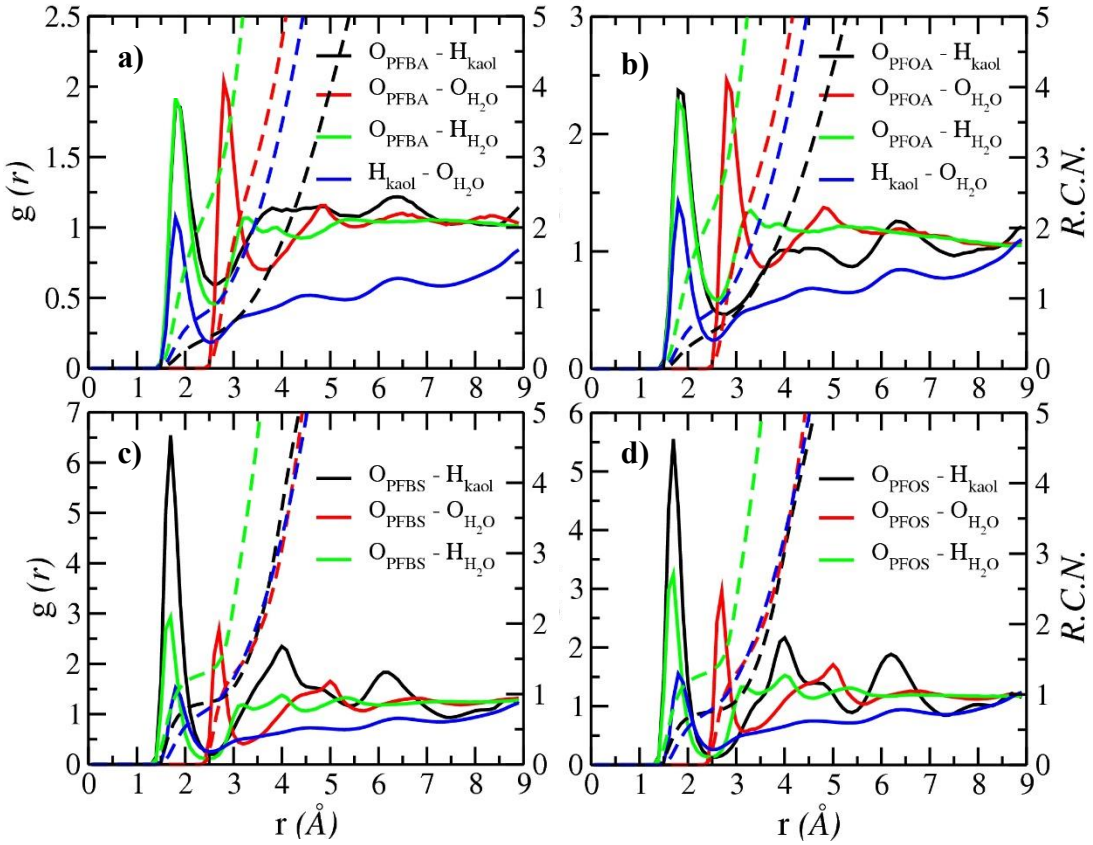

Figure 6: RDFs (solid lines) and corresponding RCNs (dashed lines) for the indicated atomic pairs at the external hydroxyl surface of Ca- kaolinite. a) PFBA, b) PFOA, c) PFBS, d) PFOS.

838 **Table 1:** Diffusion coefficients (10^{-10} m^2/s) of all PFAS and H_2O molecules at the external (001)

839 surface of different cationic kaolinite models.

Species	K- kaolinite	Ca- kaolinite	Na- kaolinite
PFBA	3.52 (3)	3.50 (1)	3.45 (2)
PFBS	0.60 (2)	0.54 (3)	0.58 (1)
PFOA	1.21 (2)	1.09 (5)	1.17 (2)
PFOS	0.32 (4)	0.29 (2)	0.33 (1)
H_2O_{PFOS}	32.01 (5)	31.92 (2)	31.75 (5)

840

841

842

843

844

845

846

847

848

849

850

851

852

Title Graphic